Radiative decay in semiconductor quantum dots at finite temperatures

J.R. Kuklinski [1] and Shaul Mukamel
University of Rochester, Chemistry Department, Rochester, NY 14627, USA

Received 20 September 1991; in final form 7 November 1991

The radiative decay rates of the lowest electronic excitations in a semiconductor sphere (quantum dot) are calculated for various temperatures and radii. We investigate how the interplay of quantum confinement and lattice vibrations affects the nature of the single electron–hole eigenstates. Application is made to the interpretation of recent fluorescence experiments in CdS quantum dots.

1. Introduction

The elementary electronic excitations in semiconductor microcrystallites are intermediate between the Wannier excitons, characteristic of bulk semiconductors, and electron–hole pairs strongly confined by a three-dimensional well [1–7]. Since the large oscillator strength carried by excitonic states is of great interest in the fabrication of materials with large nonlinear susceptibilities [7], the optical properties of materials composed of semiconductor microspheres (quantum dots) have attracted a wide attention. Previous investigations of layered semiconductor structures (quantum wells) have shown that in quasi two-dimensional systems (i.e. with one degree of freedom of electronic motion constrained by geometry), the excitonic state is much more stable against phonon disruption, since it has a larger binding energy, and the excitonic resonances may be observed even at room temperature. For realistic semiconductor microspheres with sizes comparable to, or smaller than the bulk Wannier exciton radius, R_B, the bound excitonic state is perturbed by boundary conditions and phonons, and a quantitative analysis of the relative magnitude of both effects is necessary in order to characterize its optical properties [1–11]. The confined excitonic-like one and two (electron–hole) pair states were investigated using numerical [5,6] and variational [8–10] techniques. These calculations focused on the electronic degrees of freedom, and did not take into account nuclear motions and coupling with phonons. Depending on the radius of the semiconductor microcrystallite, a transition from a discrete electronic structure characteristic of a small, molecular-like system, to the bulk is observed. The details of this transition were extensively studied experimentally using absorption, fluorescence, pump–probe and hole-burning techniques [1–7,11]. Another important problem is related to the mechanism and the magnitude of the nonlinear susceptibilities of quantum-dot microstructures, which are also largely determined by the one and two-pair states [1–11].

In this Letter, we investigate the radiative recombination of a single electron–hole pair in a spherical semiconductor particle and explore its variation with particle size and temperature. In section 2 we introduce the Hamiltonian, and in section 3 we analyze the variation of the radiative decay with size at $T=0$. We use a confined electron and hole basis set [6,7], and neglect surface effects. For very small particles, the eigenstates are close to the noninteracting electron–hole pair, and the Coulomb interaction is negligible [6,7]. In this basis, the oscillator strength is

[1] Current address: Institute for Theoretical Physics, Polish Academy of Sciences Al. Lotników 32/46, 02-668 Warsaw, Poland.

equally distributed among a few bright states. Our results show the buildup of electron–hole correlations as the radius is increased, which result in the redistribution of the oscillator strength. Phonon and temperature effects are studied in section 4. Temperature affects the radiative dynamics through phonon-induced transitions which shift population from the radiatively accessible bright states to the dark states, and therefore tend to decrease the observed radiative decay rate [12]. In the regime of temperatures where the excitonic bound state is not destroyed by coupling to phonons, the radiative decay rate increases with the radius of the microsphere, as long as the radius is smaller than the exciton coherence length. This effect is very similar to the behavior of molecular particles with Frenkel excitons [12,13]. However, for higher temperatures, the excitonic bound state is destroyed and the decay rate may decrease with dot size. The combined effect of phonons on both the relative and the center-of-mass motions of the electron–hole pairs makes the radiative decay in semiconductors a much more complex problem then the corresponding one for molecular clusters with Frenkel excitons.

2. The quantum-dot Hamiltonian

We shall be interested in the quantum dynamics of an electron–hole pair state, confined in a semiconductor sphere with radius R. The Hamiltonian is

$$H_0 = \int \mathrm{d}\boldsymbol{r}\,\hat{\psi}^+(\boldsymbol{r})\left(\frac{\hat{P}_e^2}{2m_e} + \frac{\hat{P}_h^2}{2m_e} + \hbar\omega_g + V_B(\boldsymbol{r})\right)\hat{\psi}(\boldsymbol{r}) + \int \mathrm{d}\boldsymbol{r}_1\,\mathrm{d}\boldsymbol{r}_2\,\hat{\psi}^+(\boldsymbol{r}_1)\hat{\psi}^+(\boldsymbol{r}_2)V_C(\boldsymbol{r}_1-\boldsymbol{r}_2) \times \hat{\psi}(\boldsymbol{r}_2)\hat{\psi}(\boldsymbol{r}_1)\,, \tag{1}$$

where $\hat{P}_e(\hat{P}_h)$ is the electron (hole) momentum operator, $\hbar\omega_g$ is the band gap energy, $V_C = e^2/\epsilon_0 r$ is the Coulomb potential ($r \equiv |\boldsymbol{r}|$) and V_B is the periodic potential associated with the periodic structure of the solid. e is the electronic charge and ϵ_0 is the static dielectric constant of the medium.

For the electron we use the orthonormal basis set of a particle in a spherical well, which vanishes on the surface [1,6,7]

$$\varphi_\alpha(\boldsymbol{r}) = \mathcal{N}_{nl} j_l(a_{nl} r/R) Y_{lm}(\theta,\phi)\,, \tag{2a}$$

with eigenvalues (in the effective mass approximation)

$$\epsilon_\alpha = \frac{\hbar^2 a_\alpha^2}{2m_e^2 R^2}\,, \tag{2b}$$

where α stands for the quantum numbers $\alpha = nl$; $n = 0, 1, \ldots, l = 0, \ldots, n-1$, $j_l(x)$ are the spherical Bessel functions, $Y_{lm}(\theta,\phi)$ are the spherical harmonics and a_{nl} is the nth root of the lth Bessel function [6]. Similarly, the hole basis set is given by the same functions with the electron effective mass m_e replaced by the corresponding hole mass m_h, and ϵ_α denoted ϵ'_α.

The electronic field-operator has the form

$$\hat{\psi}(\boldsymbol{r}) = \sum_\alpha \left(\hat{c}_\alpha^+ u_c(\boldsymbol{r}) + \hat{d}_\alpha^+ u_v^*(\boldsymbol{r})\right)\varphi_\alpha(\boldsymbol{r})\,, \tag{3}$$

where $\hat{c}_\alpha^+$ and $\hat{d}_\alpha^+$ denote operators creating electrons and holes, respectively, in the states with a spatial envelope $\varphi_\alpha(\boldsymbol{r})$, and where $u_v(\boldsymbol{r})$ ($u_c(\boldsymbol{r})$) is the periodic part of the Bloch function for the valence (conduction) bands. We assume that initially a single electron–hole pair is created by the absorption of a photon. Since there is no spin-flip interaction in our Hamiltonian, the electron and hole must carry opposite spins and the spin index will be omitted. We now introduce the creation operator of an electron–hole pair [14] $\hat{Y}_{\alpha\beta}^+ \equiv \hat{c}_\beta^+ \hat{d}_\alpha^+$. Making the effective mass approximation for both electrons and holes, the part of Hamiltonian given by eq. (1) describing the attraction of confined electrons and holes can be rewritten as

$$H_0 = \sum_\alpha \left[\left(\tfrac{1}{2}\hbar\omega_g + \epsilon_\alpha\right)\hat{c}_\alpha^+ \hat{c}_\alpha + \left(\tfrac{1}{2}\hbar\omega_g + \epsilon'_\alpha\right)\hat{d}_\alpha^+ \hat{d}_\alpha\right] + \sum_{\alpha\beta\alpha'\beta'} V_{\alpha\beta,\alpha'\beta'} \hat{Y}_{\alpha\beta}^+ \hat{Y}_{\alpha'\beta'}\,, \tag{4}$$

where

$$V_{\alpha\beta,\alpha'\beta'} \equiv \int \mathrm{d}\boldsymbol{r}_1\,\mathrm{d}\boldsymbol{r}_2\,\varphi_\alpha^*(\boldsymbol{r}_1)\varphi_\beta^*(\boldsymbol{r}_2) \times V_C(\boldsymbol{r}_1-\boldsymbol{r}_2)\varphi_{\alpha'}(\boldsymbol{r}_1)\varphi_{\beta'}(\boldsymbol{r}_2)\,. \tag{5}$$

In eq. (5) we neglect the dipole and higher multipoles associated with the electric field generated by a unit cell [7].

The Hamiltonian (4) can be diagonalized using the transformation

$$|\sigma\rangle = \sum_{\alpha\beta} U_{\sigma}^{\alpha\beta} d_{\alpha}^{+} c_{\beta}^{+} |\Omega\rangle , \tag{6}$$

with $|\Omega\rangle$ being the vacuum state, resulting in

$$H_0 = \sum_{\sigma} \hbar\omega_{\sigma} |\sigma\rangle\langle\sigma| . \tag{7}$$

Here $|\sigma\rangle$ denotes the Coulomb one pair eigenstates, with eigenvalues $\hbar\omega_{\sigma}$.

3. Radiative decay at $T=0$

In the dipole approximation, the coupling of the semiconductor particle to the radiation field is given by

$$H_{\text{int}} = -\hat{E}(\boldsymbol{r}, t)\hat{P} , \tag{8a}$$

where $\hat{E}$ is the electric field, and the dipole operator is given by

$$\hat{P} \equiv \int d\boldsymbol{r}\, \hat{\psi}^{+}(\boldsymbol{r}) e\boldsymbol{r} \hat{\psi}(\boldsymbol{r}) . \tag{8b}$$

The coupling to the radiation field involves both inter- and intra-band transitions [7]. In the following we neglect intraband transitions, which yields [7]

$$\hat{P} \approx \hat{P}_{\text{cv}} = d_{\text{cv}} \sum_{\alpha} (\hat{c}_{\alpha} \hat{d}_{\alpha} + \text{h.c.}) , \tag{9a}$$

where

$$d_{\text{cv}} \equiv \int d\boldsymbol{r}\, e\boldsymbol{r} u_{\text{c}}^{*}(\boldsymbol{r}) u_{\text{v}}(\boldsymbol{r}) . \tag{9b}$$

In order to obtain this result we need to go beyond the coarse grained approximation employed in the effective mass model (eq. (4)) and consider the variation of the wavefunction over a single unit cell. The key approximation is neglecting the dependence of the periodic part of the Bloch function on the k vector, i.e. we assume that the periodic parts of the Bloch functions u_{c} and u_{v} do not vary within the same band. We then decompose the integral over $\boldsymbol{r}$ into an integral over a single unit cell and a sum over unit cells, resulting in eqs. (9).

The radiative recombination rate of a single-pair state with an electron in the state α and a hole in the state β is given by the Fermi Golden Rule

$$\gamma_{\alpha\beta} = \frac{4\omega_{\text{g}}^3}{3hc^3} |\langle\Omega|\hat{P}_{\text{cv}}|\hat{Y}_{\alpha\beta}^{+}\Omega\rangle|^2 . \tag{10}$$

Using eq. (9a) we get $\gamma_{\alpha\beta} = \delta_{\alpha\beta}\gamma_0$, where

$$\gamma_0 \equiv \frac{4\omega_{\text{g}}^3 d_{\text{cv}}^2}{3hc^3} . \tag{11}$$

Similarly, the radiative decay rate of the Coulomb eigenstates is

$$\gamma_{\sigma} = \frac{4\omega_{\text{g}}^3}{3hc^3} |\langle\Omega|\hat{P}_{\text{cv}}|\hat{Y}_{\sigma}^{+}\Omega\rangle|^2 , \tag{12}$$

which can be recast in the form

$$\gamma_{\sigma} = \gamma_0 \left| \sum_{\alpha} U_{\sigma}^{\alpha\alpha} \right|^2 . \tag{13}$$

We further note that when a localized (tight binding) basis set is used, i.e. $|\sigma\rangle = \int d\boldsymbol{r}_1\, d\boldsymbol{r}_2\, \phi(\boldsymbol{r}_1, \boldsymbol{r}_2) |\boldsymbol{r}_1, \boldsymbol{r}_2\rangle$, where $|\boldsymbol{r}_1, \boldsymbol{r}_2\rangle$ denotes the one pair state with an electron localized in a unit cell with position $\boldsymbol{r}_1$ and a hole at $\boldsymbol{r}_2$, the decay rate of the single pair state can be rewritten as

$$\gamma_{\sigma} = \gamma_0 \left| \int d\boldsymbol{r}\, \phi(\boldsymbol{r}, \boldsymbol{r}) \right|^2 . \tag{14}$$

Radiative recombination can therefore be described by the effective Hamiltonian

$$H_{\text{eff}} = H_0 - \text{i} \sum_{\sigma} \gamma_{\sigma} \hat{Y}_{\sigma}^{+} \hat{Y}_{\sigma} . \tag{15}$$

In the strong confinement (small dot) limit, where the Coulomb repulsion can be neglected, the radiative rates have a simple bimodal distribution; the decay rates of single-pair states are equal to γ_0 when $\alpha = \beta$ and vanish otherwise (eq. (11)). When the Coulomb interaction is turned on, the transformation $U_{\sigma}^{\alpha\beta}$ redistributes the oscillator strength among the bright and dark zeroth-order states, as shown by eq. (13), and the distribution of decay rates is modified.

We have numerically diagonalized (4), resulting in the Coulomb eigenstates (eq. (6)) and eigenvalues and their radiative decay rates. A convenient parameter which measures the mixing induced by the Coulomb interaction is the inverse participation ratio [15]

$$Q_{\sigma}^{-1} \equiv \sum_{\alpha\beta} |U_{\sigma}^{\alpha\beta}|^4 . \tag{16}$$

When the free pair states constitute a good basis set, we have $Q_\sigma^{-1}=1$, whereas as the Coulomb interaction becomes more significant, the free pair states are heavily mixed and $Q_\sigma^{-1}\approx 0$. The variation of Q_σ^{-1} between 0 and 1 provides therefore a simple measure of the effect of Coulomb interaction on the eigenstates. The eigenvalues and Q_σ^{-1} of the lowest fifteen eigenstates of various size particles are displayed in fig. 1a. Characteristic parameters for CdS are used ($m_e=0.235m_0$, $m_h=1.35m_0$, $\epsilon_0=9$, where m_0 is the electron mass). For these parameters, the radius of the Wannier exciton is $R_B\equiv\epsilon_0\hbar^2/m_e e^2$ is 30 Å. Fig. 1 demonstrates the degree of mixing and shows that the lowest eigenstates are more strongly perturbed by the Coulomb potential. The radiative decay rates of the same states are plotted as a function of the eigenvalues E for various sizes of the microsphere in fig. 1b. In the strong confinement ($R\to 0$) limit we obtain a bimodal distribution of "bright" states ($\alpha=\beta$) with the radiative decay rate γ_0 and "dark" states ($\alpha\neq\beta$) with $\gamma=0$. As the radius of the microsphere is increased, the Coulomb attraction becomes more significant, the electron and hole motions become correlated and the oscillator strength is redistributed. The evolution of the oscillator strength distribution for increasing size of the microsphere presented on fig. 1b shows the signature of the buildup of the 1s excitonic state. Note that the effective mass approximation used here, implies the neglect of effects of anisotropy in the electron and hole mass. This anisotropy provides another mechanism for mixing the free pair states which may be significant for CdS, but is neglected here. In the bulk ($R\to\infty$) limit, the ratio of the radiative decay rates of excitonic states is governed by the value of the hydrogenic wavefunction at $r=0$ [14] i.e.

$$\frac{\Gamma_\sigma}{\Gamma_{1s}}=\frac{|\phi_\sigma(0)|^2}{|\phi_{1s}(0)|^2}, \tag{17}$$

where $\phi_{1s}(r)$ is the hydrogenic wavefunction. The

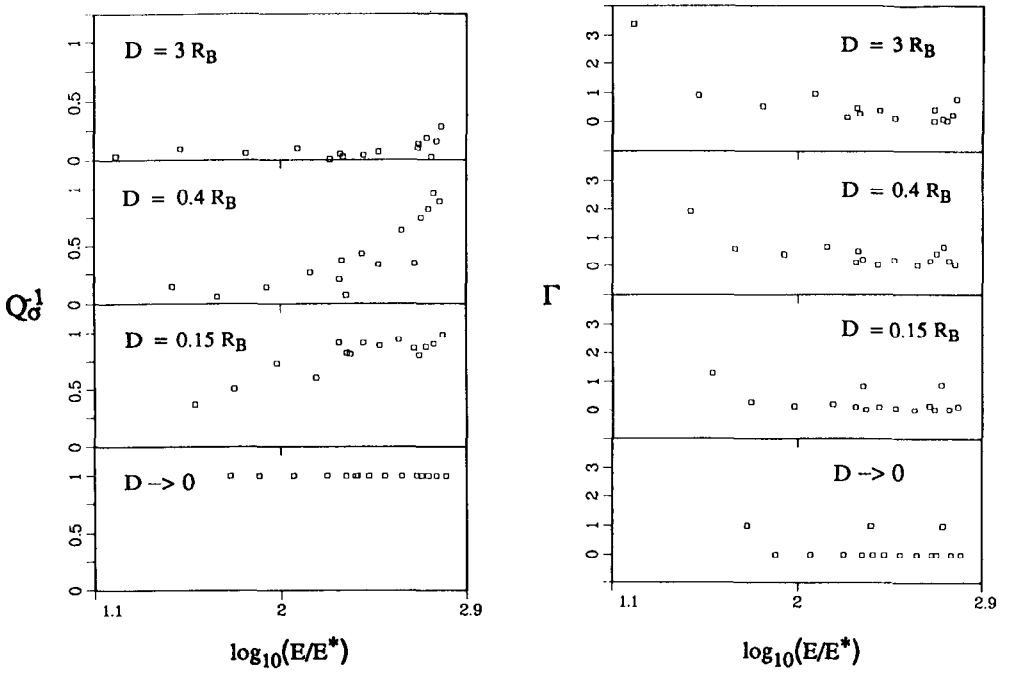

Fig. 1. (a) The inverse participation ratio Q_σ^{-1} is displayed as a function of the energy of the fifteen lowest one-pair eigenstate E for various diameters of the microsphere D. The parameters $m_e=0.235m_0$, $m_h=1.35m_0$, $\epsilon_0=9$, with m_0 the electron mass were used. For these parameters $R_B=30$ Å and the reference energy $E^*\equiv 2\pi^2\hbar^2/m_eR_B^2=4.2\times10^{-3}$ eV. Note that these states do not represent bound excitons, and all energies are therefore positive. (b) The radiative decay rate Γ is displayed as a function of the energy of the one-pair eigenstate E for various diameters of the microsphere D. Same parameters of 1a were used.

distribution of radiative decay rates in the bulk as given by eq. (17) is shown in fig. 2. Comparing it with fig.1, we note that the particle size range covered in fig. 1 is not broad enough to allow for the formation of excitons. The eigenvalues in fig. 1 are still positive and the distribution of radiative decay rates is very different from that of fig. 2. The states shown in fig. 1 should therefore be viewed as correlated electron–hole pairs rather than excitons.

The decay rate of the lowest single-pair eigenstate is plotted in fig. 3 as a function of the radius R ($T=0$ K curve). In analyzing fig. 3 we note that size confinement affects both the relative electron–hole motion as well as their center of mass. As the size is increased in the small size ($R \ll R_B$) limit, the relative motion becomes more excitonic like, and the rate is increased. For $R \gg R_B$, the size effect is mainly due to the center-of-mass motion. Following the concept of oscillator strength per unit volume [14], we expect that the decay rate of a Wannier exciton in a sphere larger than the bulk exciton radius and smaller than the wavelength should be for $T=0$ equal to $\gamma_W=\gamma_0(R/R_B)^3$. Therefore the increase observed for $T=0$ and $R>R_B$ on fig. 3 may be a signature of the expected $\sim R^3$ enhancement, i.e. of the onset of cooperative (superradiant) decay of Wannier excitons. A similar scaling was predicted and observed in Frenkel excitons [12,13].

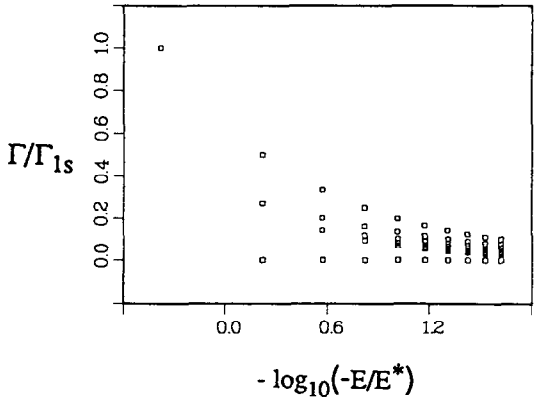

Fig. 2. The radiative decay rates of the bulk excitonic states with principal quantum number $n=1, 2, ..., 10$ and zero center-of-mass momentum, relative to the decay rate of the 1s exciton, is displayed as a function of the energy E. Note that, unlike fig. 1, these are bound excitons, and the energies are negative. Same parameters of fig. 1a are used. level degeneracies are not shown.

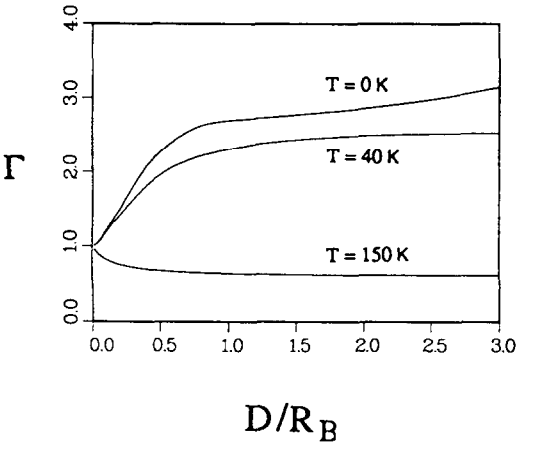

Fig. 3. The radiative decay rate Γ is displayed as a function of the quantum-dot diameter $D=2R$ for three temperatures. We used the parameters of fig. 1a together with $V_0/\gamma_0=0.15$, and $\sqrt{\kappa/\rho}R^{-1}=10^7\,s^{-1}$, $\gamma_s=10^9\,s^{-1}$ and $\delta=0.05$.

4. Radiative decay at finite temperatures

The deformation of the lattice associated with thermal vibrations creates a potential acting on electrons and holes. The Frölich model of electron–phonon coupling assumes that the lattice deformation is associated with dielectric polarization. For simplicity, we consider only the longitudinal acoustic vibrations of the material, and assume that the deformation in $\boldsymbol{r}$ is parallel to $\boldsymbol{r}$ (radical deformation) [14]. The electron–phonon coupling is then given by

$$H_{e\text{-}ph}=\lambda\int d\boldsymbol{r}_1\,d\boldsymbol{r}_2\,\hat{\psi}^+(\boldsymbol{r}_1)\hat{\psi}(\boldsymbol{r}_1)V_{e\text{-}ph}(\boldsymbol{r}_1-\boldsymbol{r}_2)\hat{\Phi}(\boldsymbol{r}_2)$$
$$+\sum_\alpha \hbar\Omega_\alpha b_\alpha^+ b_\alpha\,, \qquad (18)$$

where $\Omega_\alpha=\sqrt{\kappa/\rho}\,a_\alpha/R$ is the frequency of the acoustic vibration and we assumed a linear dependence of the frequency on the wavevector k of acoustic plane waves in the bulk i.e. $\Omega(k)=\sqrt{\kappa/\rho}\,k$. Here κ denotes the elasticity constant and ρ is the density of the medium.

The phonon field-operator has the form

$$\Phi(\boldsymbol{r})=\sum_{\alpha}(b_{\alpha}+b_{\alpha}^{+})\varphi_{\alpha}(\boldsymbol{r})\,, \tag{19}$$

where b_{α}^{+} is the operator creating phonons in the state with a spatial envelope $\varphi_{\alpha}(\boldsymbol{r})$. The electron–phonon coupling can be further expressed using the single electron–hole pair basis set

$$H_{\mathrm{e\text{-}ph}}=\lambda\sum_{\sigma\sigma'\alpha}\tilde{V}_{\sigma\sigma'\alpha}\hat{Y}_{\sigma}^{+}\hat{Y}_{\sigma'}(b_{\alpha}^{+}+b_{\alpha})+\sum_{\alpha}\hbar\Omega_{\alpha}b_{\alpha}^{+}b_{\alpha}\,, \tag{20}$$

where

$$\tilde{V}_{\sigma\sigma'\alpha}=\lambda\int \mathrm{d}\boldsymbol{r}_1\,\mathrm{d}\boldsymbol{r}_2\,\langle\sigma|\hat{\psi}^{+}(\boldsymbol{r}_1)\hat{\psi}(\boldsymbol{r}_1)|\sigma'\rangle\times V_{\mathrm{e\text{-}ph}}(\boldsymbol{r}_1-\boldsymbol{r}_2)\varphi_{\alpha}(\boldsymbol{r}_2)\,. \tag{21}$$

Our calculation of the phonon-induced dynamics of the single electron–hole pair state proceeds as follows: using the results of section 3, in the absence of phonons, we have the equations of motion:

$$-\mathrm{i}\frac{\mathrm{d}}{\mathrm{d}t}\langle\hat{Y}_{\sigma}(t)\rangle=(\omega_{\mathrm{g}}+\omega_{\sigma}-\mathrm{i}\gamma_{\sigma})\langle\hat{Y}_{\sigma}(t)\rangle\,, \tag{22}$$

where the eigenvalues ω_{σ} and the decay rates γ_{σ} were calculated in section 3. We next evaluate numerically the electron–phonon coupling matrix elements in the Coulomb basis set $\tilde{V}_{\sigma\sigma'\alpha}$. The electron–phonon coupling potential is assumed to have a Frölich form [14] (η is a polarizability constant):

$$V_{\mathrm{e\text{-}ph}}(\boldsymbol{r}-\boldsymbol{r}')\varphi_{\alpha}(\boldsymbol{r}')=-\frac{\eta e}{\epsilon_0}\frac{1}{|\boldsymbol{r}-\boldsymbol{r}'||\boldsymbol{r}'|}\,\boldsymbol{r}'^{*}\nabla_{\boldsymbol{r}'}\varphi_{\alpha}(\boldsymbol{r}'')\,. \tag{23}$$

In the numerical calculations reported here, we have approximated the coupling by

$$V_{\mathrm{e\text{-}ph}}(\boldsymbol{r}-\boldsymbol{r}')\varphi_{\alpha}(\boldsymbol{r}')\approx-\frac{V_0[\varphi_{\alpha}(\boldsymbol{r}'(1+\delta))-\varphi_{\alpha}(\boldsymbol{r}')]}{R^3\delta(|\boldsymbol{r}-\boldsymbol{r}'||\boldsymbol{r}'|+\delta R^2)}\,. \tag{24}$$

Since the electron–phonon coupling scales as the inverse volume of the particle, we have introduced the scaled coupling parameter $V_0\equiv(\eta e/\epsilon)R^3$ which does not change with R. δ is a dimensionless parameter used to improve the numerical convergence. Eq. (24) reduces to eq. (23) as $\delta\to 0$.

The present model of electron–phonon coupling (eq. (24)) together with the linear dispersion relation for phonons, represents the impact of acoustic phonons on the radiative decay process. In general, both acoustic and optical phonons should be considered, and their interaction with electrons is usually modelled using both the contact and Frölich-type of interactions [14].

The radiative decay time profile was calculated by following the time-dependent populations of the Coulomb states. To that end we introduce the variables representing these populations

$$G_{\sigma}(t)\equiv\langle\hat{Y}_{\sigma}^{+}(t)\hat{Y}_{\sigma}(t)\rangle\,. \tag{25}$$

The time-dependent photon emission rate is then given by

$$I(t)=\sum_{\sigma}\gamma_{\sigma}G_{\sigma}(t)\,. \tag{26}$$

The time-dependent excited state populations were calculated using the following master equation:

$$\frac{\mathrm{d}}{\mathrm{d}t}G_{\sigma}(t)=D_{\sigma\sigma}G_{\sigma}(t)+\lambda^2\int_0^{\infty}\mathrm{d}\tau\sum_{\sigma'}W_{\sigma\sigma'}(\tau)G_{\sigma'}(t-\tau)\,, \tag{27}$$

where

$$D_{\sigma\sigma'}=\mathrm{i}(\omega_{\sigma}-\omega_{\sigma'})-\gamma_{\sigma}-\gamma_{\sigma'}\,, \tag{28}$$

and the Laplace transform of the transition rate from state σ' to σ is given by

$$W_{\sigma\sigma'}(z)=\sum_{\alpha}(1-\delta_{\sigma\sigma'})|\hat{V}_{\sigma\sigma\alpha}|^2\times\left(\frac{n_{\alpha}}{z+D_{\sigma\sigma'}-\mathrm{i}\Omega_{\alpha}-\gamma_{\alpha}}+\frac{n_{\alpha}+1}{z+D_{\sigma\sigma'}+\mathrm{i}\Omega_{\alpha}-\gamma_{\alpha}}\right)+\delta_{\sigma\sigma'}\sum_{\alpha\sigma''}|\tilde{V}_{\sigma\sigma''\alpha}|^2\times\left(\frac{n_{\alpha}}{z+D_{\sigma\sigma''}-\mathrm{i}\Omega_{\alpha}-\gamma_{\alpha}}+\frac{n_{\alpha}+1}{z+D_{\sigma\sigma''}+\mathrm{i}\Omega_{\alpha}-\gamma_{\alpha}}\right). \tag{29}$$

z is the Laplace variable conjugate to t and $n_{\alpha}=[\exp(\hbar\Omega_{\alpha}/kT)-1]^{-1}$ is the Boson thermal occupation number of the α mode. The master equation was derived by starting with the Heisenberg equations, and the derivation is similar to our pre-

vious derivation for molecular aggregates [12]. We have employed the factorization

$$\langle \hat{b}^{+}_{\alpha}(t)\hat{b}_{\alpha'}(t-\tau)\hat{Y}^{+}_{\sigma}(t-\tau)\hat{Y}_{\sigma}(t-\tau)\rangle \approx \langle \hat{b}^{+}_{\alpha}(t)\hat{b}_{\alpha'}(t-\tau)\rangle\langle \hat{Y}^{+}_{\sigma}(t-\tau)\hat{Y}_{\sigma}(t-\tau)\rangle , \quad (30)$$

where the phonons are assumed to be unperturbed by the electronic motion so that

$$\langle \hat{b}^{+}_{\alpha}(t)\hat{b}_{\alpha'}(t')\rangle = \delta_{\alpha\alpha'} n_{\alpha} \exp[-i\Omega_{\alpha}(t-t')-\gamma_{s}|t-t'|] . \quad (31)$$

γ_s is the phonon damping rate. We also neglected the coupling between diagonal ($\langle \hat{Y}^{+}_{\sigma}(t)\hat{Y}_{\sigma}(t)\rangle$) and nondiagonal ($\langle \hat{Y}^{+}_{\sigma}(t)\hat{Y}_{\sigma'\neq\sigma}(t)\rangle$) terms of the electronic density matrix (this is exact for periodic boundary conditions).

The solution of eq. (27) can be written in Laplace space as

$$G_{\sigma}(z)=\sum_{\sigma'}[z\hat{I}-\hat{D}-\lambda^{2}\hat{W}(z)]^{-1}_{\sigma\sigma'}G_{\sigma'}(t=0) . \quad (32)$$

We further assume that at $t=0$ an electron–hole pair is created in the lowest eigenstate $|\sigma\rangle$. This state corresponds for a microsphere larger than the Wannier exciton radius to the 1s exciton with zero center-of-mass momentum, whereas in the strong confinement limit this is the 1s–1s single-pair state. We therefore use the initial condition $G_{\sigma}(t=0)=\delta_{\sigma,1}$. The slowly varying part of time dependent population of various single-pair states is evaluated from

$$G_{\sigma}(z)=[z\hat{I}-\hat{D}-\lambda^{2}\hat{W}(z)]^{-1}_{\sigma\sigma'=1} , \quad (33)$$

using a method described in ref. [12], which consists of approximating $\hat{W}(z)\approx\hat{W}^{0}+z\hat{W}^{1}$ in order to find the poles lying close to $z=0$, we obtained a solution of the form $G_{\sigma}(z)=\sum_{n}a_{n}(z-b_{n})$. We then calculated numerically the average radiative decay time τ_R defined by

$$1-1/e\equiv\int_{0}^{\tau_R} dt\, I(t) \quad (34)$$

(i.e. τ_R is the time in which the total probability of emitting a photon is equal to $1/e$). We then define a dimensionless radiative decay rate $\Gamma\equiv(\tau_R\gamma_0)^{-1}$.

The dynamics of $G_{\sigma}(t)$ was solved numerically using this method. We have used the same typical parameters for CdS (ϵ_0, m_e and m_h) used in figs. 1 and 2. The excitonic Bohr radius for these parameters is equal to $R_B\approx 30$ Å. We reiterate that the present calculation does not include the anisotropy of the effective mass or the light and heavy hole structure. The parameters $\sqrt{\kappa/\rho}\,R^{-1}=10^{7}$ s^{-1} and $V_0/\gamma_0=0.15$ were chosen to fit the data of ref. [16] (see fig. 4). The value of γ_0 corresponding to this fit is $\gamma_0\approx 4\times10^{10}$ s^{-1}. In the numerical calculations we have used the parameters $\gamma_s=10^{9}$ s^{-1} and $\delta=0.05$. These parameters were adjusted to assure the numerical stability of the computed radiative decay rates.

We found the solution of the master equation (eq. (27)) to be numerically unstable unless the phonon damping γ_s exceeded a value of $\gamma_s\approx10^{9}$ s^{-1}. Above this value, the solution was practically independent of γ_s when it was varied by two orders of magnitude. γ_s should thus be viewed as a smoothing (coarse graining over time) parameter. We have checked the validity of our calculations by extending the second-order expression for $W_{\sigma\sigma'}$ (eq. (29)) to fourth order. The fourth-order master equation (which is considerably more complicated) is numerically stable and the results (with $\gamma_s=0$) agreed with those obtained using the present second-order calculation with the smoothing parameter γ_s. This confirms the convergence of the present procedure.

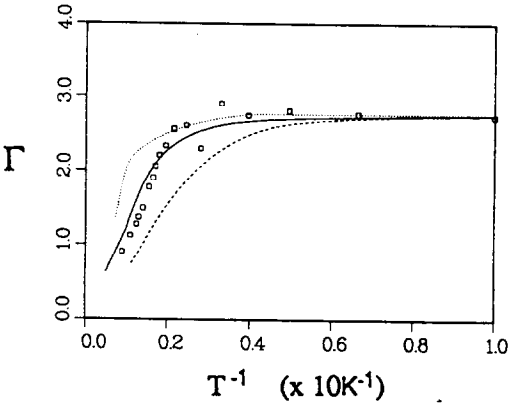

Fig. 4. The radiative decay rate Γ is displayed as a function of temperature. The various curves represent different values of $V_0/\gamma_0=0.15$ (——), 0.1 (– – –), 0.2 (···). The dot radius is $R=20$ Å. Other parameters are same as in fig. 3. The squares represent the experimental results [16] coming from fluorescence studies in the 5–100 K temperature range in CdS.

In fig. 3 we display the calculated effective decay rate as a function of the microsphere radius for several temperatures. We see that for $T=0$ K the dependence of Γ on the radius of the microsphere reflects the buildup of the 1s excitonic state. For increasing radius, the confinement effect of electron and hole states is overcome by the attractive Coulomb potential which increases the correlation between the electron and the hole, leading to a faster radiative recombination rate. A different behavior is observed for $T=150$ K, where the decay rate is decreasing for larger sizes of the microsphere. This can be viewed as a consequence of the decreased splitting among various electronic levels, which facilitates phonon mediated transitions. If the concept of oscillator strength per unit volume [17] is applied together with the temperature-dependent coherence length [12], we expect that the decay rate of a Wannier exciton in a sphere larger than the bulk exciton radius and smaller than the wavelength should be equal to $\gamma_W=\gamma_0(R_c(T)/R_B)^3$, where R_c is the coherence length associated with the center-of-mass motion. This scaling is completely analogous to that found for Frenkel excitons [12,13].

Recent fluorescence experiments performed on CdS particles with 30–50 Å diameters, have measured the radiative decay rate in the temperature range 5–100 K. The fluorescence of semiconductor particles is usually dominated by trapped states (e.g. at the surface), and does not provide a direct measure of the radiative lifetime [2]. These experiments, however, had employed high quality samples which show a relatively intense band-edge emission compared with the red-shifted emission from trapped states. The short time dynamics is therefore believed to reflect the purely radiative decay [16]. We have compared the predictions of our theory to these experiments. The solid curve in fig. 4 shows the decay rate Γ as a function of the inverse temperature. The squares show the experimental data [16] (the parameters κ, γ_0 and V_0 were fitted to these data). The dotted and dashed lines show the decay rate for different values of the electron–phonon coupling strength (V_0). The dependence on V_0 displayed in fig. 4 has a simple intuitive interpretation; stronger electron–phonon coupling more rapidly destroys the cooperative emission, and reduces the decay rate Γ. The various curves in fig. 4 demonstrate the sensitivity of the average radiative decay rate to the electron–phonon coupling strength.

5. Summary

We have calculated the lifetime of single-pair electron–hole states in a semiconductor sphere. The calculations were made by neglecting the effects of surface states, the nonparabolicity and nonuniformity of bands in semiconductors, the lattice vibrations with nonradial displacement, and using a simplified phonon structure with LA modes only. We have shown that the suppression of the radiative decay at finite temperatures may be viewed as a consequence of phonon-induced mixing between short and long-lived electron–hole states.

Radiative recombination in semiconductor particles is much more complex than that of molecular clusters with Frenkel excitons. In the latter problem, the exciton motion can be characterized by a single coherence length which controls the extent of cooperativity in the radiative decay [12]. For Wannier excitons we need consider both the relative and the center-of-mass motions of the electron–hole pair. The effect of confinement and coupling with phonons on both coordinates plays an important role in determining the magnitude of optical nonlinearities of semiconductor particles as of well as conjugated polymers [18]. The calculations presented here show how phonons couple with both types of degrees of freedom, and how dephasing determines a coherence length associated with the center of mass [12], as well as destroys the correlations in the relative motion of electrons and holes.

Acknowledgement

We wish to thank Professor T. Kobayashi for making the results of ref. [16] available to us prior to publication. We also wish to thank Dr. L. Brus for most useful discussions. The support of the National Science Foundation, the Center for Photoinduced Charge Transfer, and the Air Force Office of Scientific Research, is gratefully acknowledged.

References

[1] Al.L. Efros and A.L. Efros, Fiz. Tekh. Poluprovodn. 16 (1982) 1209 (Sov. Semicond 16 (1982) 772).

[2] M. Bawendi, M.L. Steigerwald and L. Brus, Ann. Rev. Phys. Chem. 44 (1990) 21.

[3] S. Schmitt-Rink, D.A.B. Miller and D.S. Chemla, Phys. Rev. B 35 (1987) 8113.

[4] P. Roussignol, D. Ricard, C. Flytzanis and N. Neuroth, Phys. Rev. Letters 62 (1989) 312.

[5] Y.Z. Hu, S.W. Koch, M. Lindberg, N. Peyghambarian, R. Pollock and F.F. Abraham, Phys. Rev. Letters 64 (1990) 1805.

[6] Y.Z. Hu, M. Lindberg and S.W. Koch, Phys. Rev. B 42 (1990) 1713;
S.H. Park, R.A. Morgan, Y.Z. Hu, M. Lindberg, S.W. Koch and N. Peyghambarian JOSA B7 (1990) 2097.

[7] S. Koch and H. Haug, Quantum theory of the optical and electronic properties of semiconductors (World Scientific, Singapore, 1990).

[8] Y. Kayanuma, Phys. Rev. B 38 (1988) 9797;
Y. Kayanuma and H. Momiji, Phys. Rev. B 41 (1990) 10261.

[9] J.B. Xia, Phys. Rev. B 40 (1989) 8500.

[10] T. Takagahara, Phys. Rev. B 39 (1989) 10206.

[11] T. Itoh, T. Ikehara and Y. Iwabuchi, J. Luminescence 45 (1990) 29.

[12] F.C. Spano, J.R. Kuklinski and S. Mukamel, Phys. Rev. Letters 65 (1990) 211; J. Chem. Phys. 94 (1991) 7534.

[13] H. Fidder and D.A. Wiersma, Phys. Rev. Letters 66 (1991) 1501.

[14] A. Stahl and I. Balslev, Electrodynamics of the semiconductor band edge (Springer, Berlin, 1987).

[15] E.N. Economou, Green's functions in quantum physics (Springer, Berlin, 1983).

[16] K. Misawa, H. Yao, T. Hayashi and T. Kobayashi, J. Chem. Phys. 94 (1991) 4131.

[17] J. Feldmann, G. Peter, E.O. Göbel, P. Dawson, K. Moore, J. Foxon and R.J. Elliot, Phys. Rev. Letters 59 (1987) 2337.

[18] H.X. Wang and S. Mukamel, to be published.